JTTEE5 16:873–880
DOI: 10.1007/s11666-007-9109-5
1059-9630/$19.00 © ASM International

Influence of Annealing on Photocatalytic Performance and Adhesion of Vacuum Cold-Sprayed Nanostructured TiO_2 Coating

Guan-Jun Yang, Chang-Jiu Li, Sheng-Qiang Fan, Yu-Yue Wang, and Cheng-Xin Li

(Submitted March 12, 2007; in revised form June 10, 2007)

Composite powder was prepared using primary nanoTiO_2 powder and polyethylene glycol (PEG). The nanoTiO_2 coating was deposited through vacuum cold spray using both the composite powder and the primary nanopowder. The influence of annealing on the coating adhesion and photocatalytic activity was investigated. The coating adhesion was evaluated through erosion test by water jet. The photocatalytic performance of the coatings was evaluated through photodegradation of phenol in water. Results showed that annealing of the coating at a temperature from 450 to 500 °C yielded both higher activity and better adhesion. The adhesion of the coating deposited using the composite powder was better than that using the primary nanoTiO_2 powder. It was found that the TiO_2 coating, resulting from the composite powder, presented much higher activity than that deposited with the primary nanopowder. The better activity is attributed to the existence of large pores resulting from the stacking of composite powder, which benefits the reactants' transportation through the porous coating.

Keywords adhesion, annealing treatment, nanocrystalline material, photocatalyst, TiO_2, vacuum cold spray

1. Introduction

Nanostructured TiO_2 coatings are of industrial importance owing to its promising applications to photocatalytical, electrical, optical, and tribological coatings (Ref 1-8). TiO_2 photocatalysis attracted much research attention in the past decades due to the environmental problem all over the world. TiO_2 photocatalysis is an attractive low-temperature, energy-saving approach, and it has promising applications to the destruction of environmental chemical contaminants, such as wastewater treatment and air purification (Ref 1, 2).

TiO_2 coatings are formed through immobilizing nanoTiO_2 particles on an inert substrate. Nanoparticles are often fixed on the support using some binders, such as glue and various solutions (Ref 8). The adherence of the coating to the support is essential for successful applications, since catalyst particles may be detached from the support if the adhesion is not strong enough. Annealing treatment from 500 to 700 °C is often utilized to improve the adherence of nanoTiO_2 particles (Ref 8). However, owing to the change of the surface microstructure of photocatalyst powders, the immobilization processing of photocatalyst powders at too high temperature generally deteriorates photocatalytic activity; therefore, it is of significant importance to transfer the photocatalytic activity of the starting powder to coating. On the other hand, since the photocatalytic performance is a kind of surface property, the microporous coating presents a higher photocatalytic performance owing to its larger surface area than compact coating. Consequently, a photocatalytic coating with micropores or nanopores is of essential interest.

Thermal spray technique, which was widely used to produce large and cost-effective high-performance coatings in ceramic, metal, and cermet, was introduced to deposit TiO_2 photocatalytic coatings. For example, plasma spray, high-velocity oxy-fuel (HVOF) spray, and cold spray were employed to fabricate the nanostructured TiO_2 photocatalyst by using agglomerated TiO_2 powder from nanoTiO_2 particles (Ref 9-15). Liquid flame spray and suspension plasma spray were used to deposit nanoTiO_2 coatings by using liquid feedstocks in both solution and suspension (Ref 11, 12, 16-19). However, in most of the study there was a high temperature effect on the spray feedstock, which may lead to the phase transformation from anatase to rutile (Ref 9-14). Although it was reported that the high-temperature flame can be avoided for TiO_2 coating deposition by conventional cold spray, it

This article is an invited paper selected from presentations at the 2007 International Thermal Spray Conference and has been expanded from the original presentation. It is simultaneously published in *Global Coating Solutions, Proceedings of the 2007 International Thermal Spray Conference*, Beijing, China, May 14-16, 2007, Basil R. Marple, Margaret M. Hyland, Yuk-Chiu Lau, Chang-Jiu Li, Rogerio S. Lima, and Ghislain Montavon, Ed., ASM International, Materials Park, OH, 2007.

Guan-Jun Yang, Chang-Jiu Li, Sheng-Qiang Fan, Yu-Yue Wang, and **Cheng-Xin Li**, State Key Laboratory for Mechanical Behavior of Materials, Xi'an Jiaotong University, Xi'an, Shaanxi 710049, P.R. China; and **Guan-Jun Yang**, School of Materials Science and Engineering, Xi'an Jiaotong University, Xi'an, Shaanxi 710049, P.R. China. Contact e-mail: ygj@mail.xjtu.edu.cn.

is much difficult to deposit thick coating with a thickness more than 10-15 μm (Ref 15).

In this study, vacuum cold spray, which was employed to deposit functional ceramic coatings at room temperature (Ref 20-22), was utilized to deposited TiO_2 coatings of nanoporous structure. The influence of annealing treatment on the photocatalytic activity and adhesion was investigated with an aim at the optimization of coating preparation. The pore size was controlled by spray powder type. The impact of pore size on photocatalytic performance was discussed based on the experiments.

2. Experimental

2.1 Materials

Commercial P25 TiO_2 nanoparticles (Degussa, Germany) in a diameter of 25 nm were used for coating deposition. Composite powder made from TiO_2 and polyethylene glycol (PEG) was prepared according to our previous results (Ref 7). The content of PEG in the powder was 37.5 wt.%. Primary P25 nanopowder was also used as a spray feedstock to deposit TiO_2 coating. A commercial glass (3 mm, Shaanxi, China) was employed as a substrate for coating deposition. Prior to spraying, the substrate was cleaned in acetone under ultrasonic.

2.2 Coating Deposition and Postannealing Treatment

The deposition of TiO_2 coating was performed using a home-developed vacuum cold spray system (Ref 7). The system was constituted of a vacuum chamber and vacuum pump, powder feeder, accelerating gas feeding unit, particle accelerating nozzle, two-dimensional worktable, and control unit. The acceleration of TiO_2 particles was performed by high-pressure He gas. Spray parameters are given in Table 1. To avoid the coating thickness effect on the photocatalytic performance, the thickness of all coatings was controlled to be more than 20 μm. The as-sprayed coatings were annealed to remove the PEG in the coating and improve the adherence between the coating and substrate. The deposited TiO_2 coatings were annealed at different temperatures from 300 to 600 °C for 30 min with a heating rate of 3 °C/min.

2.3 Characterization of Coating Microstructure

The topographical morphology was examined using field emission scanning electron microscopy (FESEM) (JSM-6700F, Tokyo, Japan). The crystalline structure of P25 powder and coatings was characterized using x-ray diffraction (XRD) system (Rigaku D/max-2400, Tokyo, Japan). XRD analysis was carried out using Cu-Kα radiation at 40 kV and 100 mA. Scan speed for 2θ was 5°/min during test. The anatase content in the as-received and annealed P25 was calculated by using diffraction intensity of rutile peak (110) and anatase peak (101), respectively, in the XRD pattern (Ref 9, 10). Peak area was used to estimate the anatase content in the nanostructured coating using the following equation (Ref 17, 18):

$$C_A = \frac{A_A}{A_A + 1.265 \cdot A_R} \cdot 100\% \quad \text{(Eq 1)}$$

where C_A is the anatase content in the TiO_2, and A_R and A_A are the areas covered by rutile peak (110) and anatase peak (101), respectively, in the XRD pattern. The grain sizes were estimated using Scherrer equation (Ref 17, 18). The porosity and pore size of TiO_2 coating and powder were measured using a nitrogen adsorption-desorption apparatus (Coulter SA 3100 plus, Beckman Coulter). The specific surface area was estimated using the BET equation, and the Barret-Johner-Halenda (BJH) treatment was applied to the isotherm in order to calculate the pore size distribution. Only small pores below 100 nm can be measured by nitrogen adsorption-desorption apparatus, and larger pores were investigated by SEM observation of the topographical morphology.

Table 1 Vacuum cold spray parameters

Chamber pressure, Pa	2×10^3
Pressure of the powder feeder gas, Pa	1×10^6
He gas flow, L/min	3
Distance from nozzle exit to substrate, mm	5
Orifice size of nozzle, mm × mm	2.5×0.2
Substrate traverse speed, mm/s	5

2.4 Evaluation of the Coating Adhesion

The adhesion between the coating and the glass substrate was evaluated by water jet erosion test. A water jet at a velocity of 8.5 m/s was projected on the coating surface perpendicular to the coating during the erosion test. The diameter of the water jet was 2 mm. Duration time of the water jet projected on the coating was 1 min. In addition, the adhesion was also examined by ultrasonic cleanout. Coatings were put in a 100 W ultrasonic cleaner for 1 min. The adhesion was evaluated according to spalling state of the coating.

2.5 Evaluation of the Photocatalytic Performance

Analytically pure phenol was employed as an aqueous organic pollutant to evaluate photocatalytic activity. The initial concentration of phenol in the solution was 5 mg/L. An annular photoreactor shown in Fig. 1 was employed in this study. It consisted of glass tube, magnetic stirrer, air bubbler, and light source. A 300 mm high glass tube having an inner diameter of 60 mm was employed as the photoreactor. To carry out the photodegradation 250 ml phenol solution was filled in the reactor. A sample coated with TiO_2 was fixed into the solution. A magnetic stirrer was placed at the reactor's bottom so that a homogenous phenol solution could be maintained in the reactor tube throughout the reaction. Airflow at a flux of 400 mL/min was bubbled in the solution to supply oxygen for the photoreaction. A cooling air was also supplied at the side of the reactor tube such that the experimental temperature was maintained at 28 ± 3 °C. A high-pressure mercury

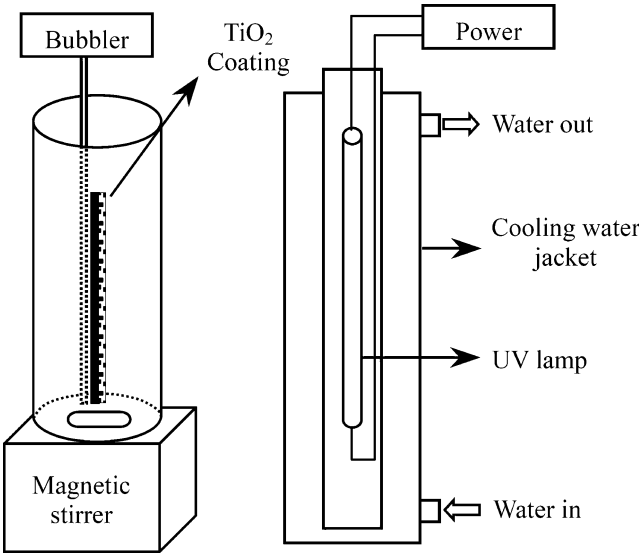

Fig. 1 Schematic diagram of the photoreactor

lamp with a primary emission wavelength at 360 nm was used as UV source. The lamp was positioned inside a cylindrical glass vessel that served as a circulating water jacket to cool the lamp. UV light was filtered at $\lambda \geq 330$ nm by the glass walls of the jacket, and infrared irradiation was also absorbed by the cooling water. The radiant flux at the coating surface was 2.93 mW/cm^2. The UV absorption spectrum of TiO_2 slurry was measured by a double-beam ultraviolet-visible spectrometer (Shimadzu UV-2401, Kyoto, Japan), in which a 10 mm thick cell was employed. The concentration of phenol was measured quantitatively through the UV spectrum obtained by the spectrometer.

3. Results

3.1 Influence of Annealing on the Coating Microstructure

Figure 2 shows the topographical morphology of the as-sprayed coating and the annealed coating at a temperature of 450 °C. The coating was deposited using the composite powder. The examination of the as-sprayed coating and annealed coating at a low magnification, shown in Fig. 2(a) and 2(c), reveals that the coatings presented a rough surface morphology. It is clearly found from Fig. 2(b) that the as-sprayed TiO_2 coating was composed of aggregated powders in diameter from 0.5 to 3 μm. The primary nanoTiO_2 in each powder was aggregated by PEG. It can be found that after annealing no significant change occurred to the surface morphology observed at a low magnification. From the surface morphology shown in Fig. 2(d), the primary nanoparticles were still well agglomerated together after the removing of PEG. Evidently, large pores, which were pointed out by arrows in Fig. 2(d), between the aggregated powders were well retained in the TiO_2 coating after annealing treatment. The size of those pores was mainly in a range from 0.2 to 1 μm.

Figure 3 shows the topographical morphology of the as-sprayed coating deposited with primary P25 nanoparticles. The coating presents a little rough surface morphology similar to that deposited with the composite powder. The detailed examination at a high magnification, shown in Fig. 3(b), demonstrates a much different topographical morphology. The coating surface was much smoother than that deposited with the composite powder. There were few pores in size of micrometer scale in the coating.

BET measurement results showed that the typical specific surface area of the primary P25, the coating deposited with P25 annealed at 600 °C and the coating deposited with composite powder annealed at 450 °C were 56, 55.9, and 53.7 m^2/g, respectively. There were small pores in a range from 5 to 40 nm in the P25 powder and all coatings. The porosity is similar to each other and in the range from 0.24 to 0.31 mL/g.

To investigate the influence of annealing treatment on the crystalline structure of P25 in the coating, the crystalline structure of the as-received P25 and annealed P25 powder was examined. Figure 4 shows the XRD patterns of the as-received P25 powder and the P25 powder annealed at 500 °C and 600 °C. The as-received P25 powder was composed of 85% anatase phase and 15% rutile phase. The estimation on the phase structure of the annealed P25 revealed that there was no difference in the anatase content of the as-received P25 from annealed P25. It was also found that the grain size in P25 powder was not influenced by annealing treatment when the annealing temperature was lower than 600 °C. It means that crystalline structure of the coating was also not influenced by annealing treatment below 600 °C.

3.2 Effect of Annealing on the Adhesion of Coatings on Substrate

Results on the water jet erosion test suggested that all coatings adhered to the substrate well enough to endure the erosion by high-speed water jet. No difference was found for the preannealing coatings and annealed coatings. Figure 5 shows the surface morphology of the coatings annealed at different temperature after ultrasonic cleaning. For the coatings deposited with the composite powder, the spalling of a fraction of coating in flake occurred to the coatings annealed at temperatures of 300 °C and 400 °C. However, little spalling occurred to the coatings annealed at temperatures of 450 °C and 500 °C. Moreover, most of the coating deposited directly with the primary P25 nanopowder flaked off the substrate.

3.3 Influence of Annealing on the Photocatalytic Performance

Figure 6 shows the change of phenol concentration with the radiation time. The result for blank reaction by using UV without TiO_2 coating is shown in Fig. 6 for comparison. When there was no coating in the reactor,

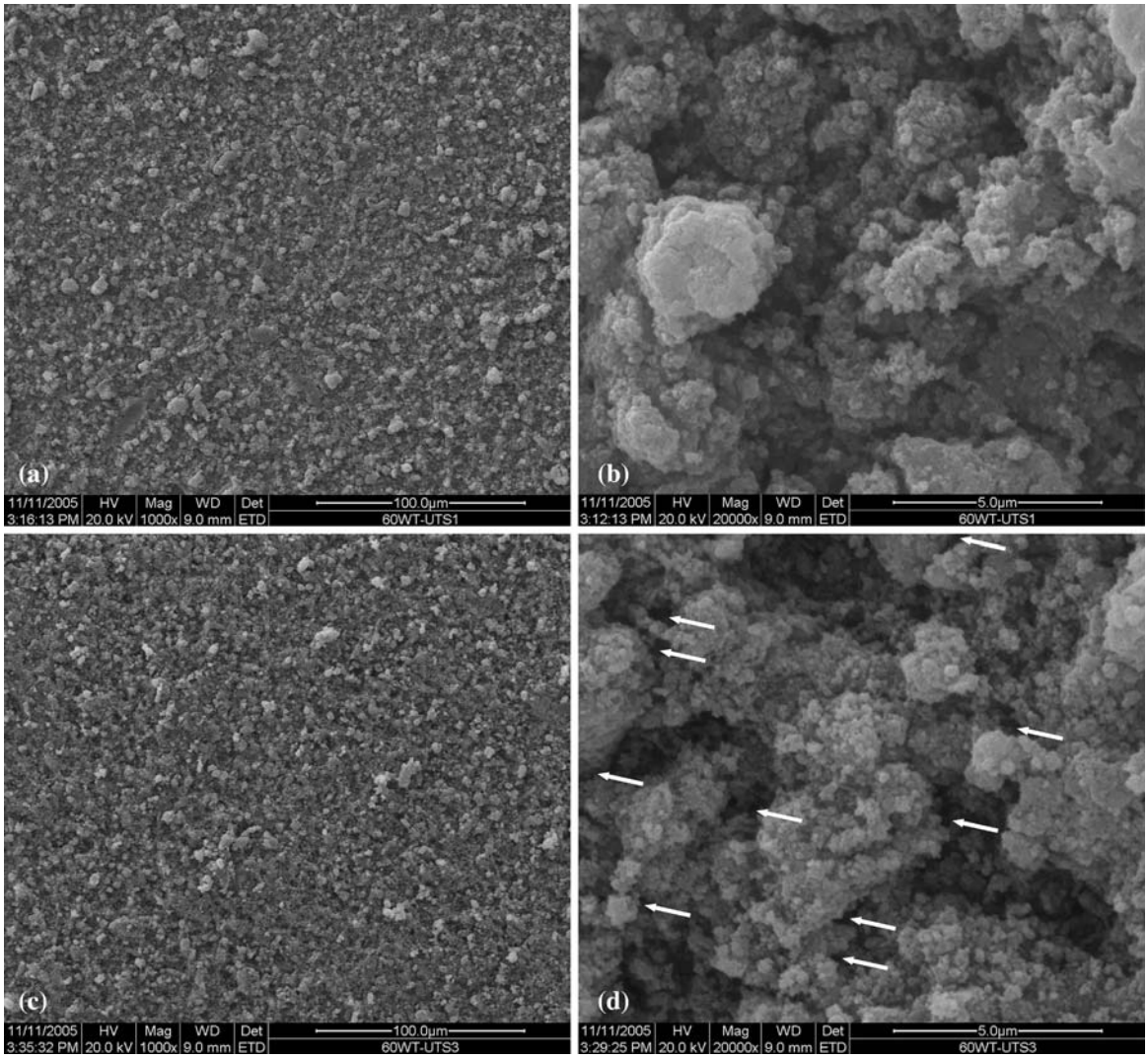

Fig. 2 Topographical morphology of the as-sprayed coating and the annealed coating at temperature of 450 °C deposited using the composite powder. (a) and (b) are referred to the as-sprayed coating; (c) and (d) to the annealed coating

phenol concentration decreased with the reaction time due to the photolysis of the phenol by the UV illumination. Five per cent of the phenol was decomposed by photolysis in 400 min. By using the TiO_2 coating annealed at 450 °C deposited with the composite powder, more than 90% of the phenol was decomposed in 350 min. This result indicates that the photocatalytic degradation of the phenol was much more significant than the photolysis; therefore, the photolysis of the phenol by UV illumination can be ignored in this study. The photocatalytic activity was evaluated by the degradation rate, which can be obtained through linearly fitting the change of phenol concentration with reaction time. Figure 7 shows the effect of annealing temperature on the activity. The activity of the coating deposited with primary P25 nanoparticles and then annealed at 600 °C was also shown in Fig. 7 for comparison. The activity of the coatings deposited with the composite powder was significantly enhanced by annealing treatment at a temperature of 450 °C. When annealing temperature was higher than 450 °C, the activity was decreased with the further increase of annealing temperature. For the coatings annealed at 600 °C, it is clearly found that the coating deposited with the composite powder was much more active than that with primary P25.

4. Discussion

The vacuum cold-sprayed TiO_2 coating deposited with the composite powder was stacked of the composite powders in size of submicrometer. Because the primary nanoparticles were bonded to each other by PEG, the individual composite powders were of a dense structure. The pores in size of 0.2-1 μm in the coatings resulted from the incompletely filling of the composite particles to rough surface valley during the powder stacking; therefore, the

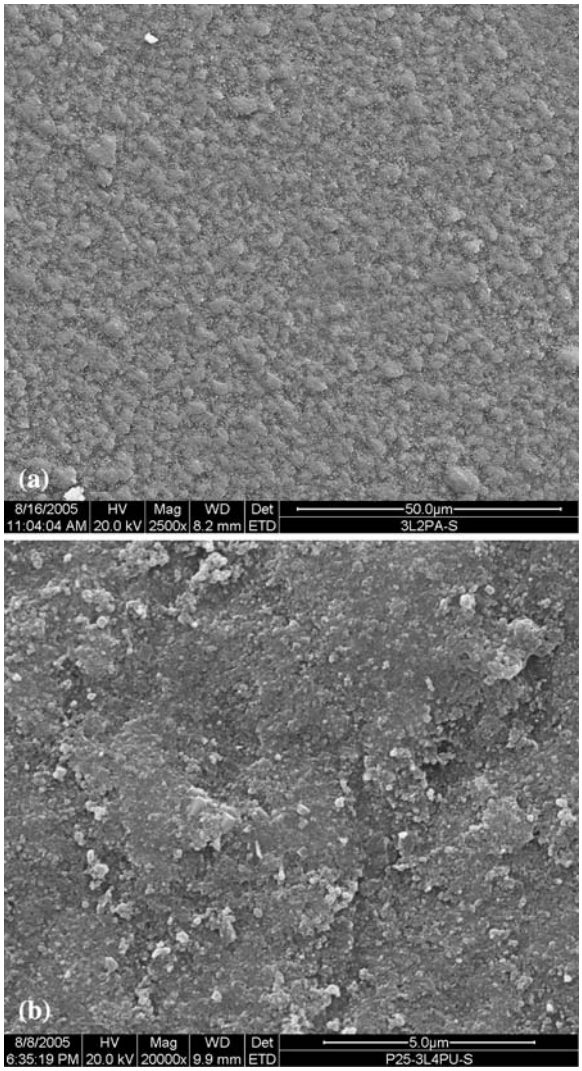

Fig. 3 Topographical morphology of the as-sprayed TiO_2 coating deposited with the primary P25 TiO_2

size of those pores was in the same scale as the size of the composite powder. When the coating was annealed at temperature higher than 300 °C, PEG in the coating was removed. The removing of PEG resulted in small pores in a size scale comparable to P25 nanoparticle size. These small pores were measured to be mainly from 5 to 40 nm. As a result, the size of pores in the annealed coatings would present bimodal distributions including nanometer scale and submicrometer scale. The large pores in submicrometer scale were originated from the loose stacking of the composite powders and existed among composite powders in size of micrometer. The small pores in nanometer scale existed among primary nanoparticles in size of nanometer.

With primary P25 nanoparticles as feedstock, the coating was composed of naturally agglomerated particles with primary nanoparticles. When an agglomerated particle impacts on a substrate surface, the powder is easily deformed due its low strength. The deformation will lead

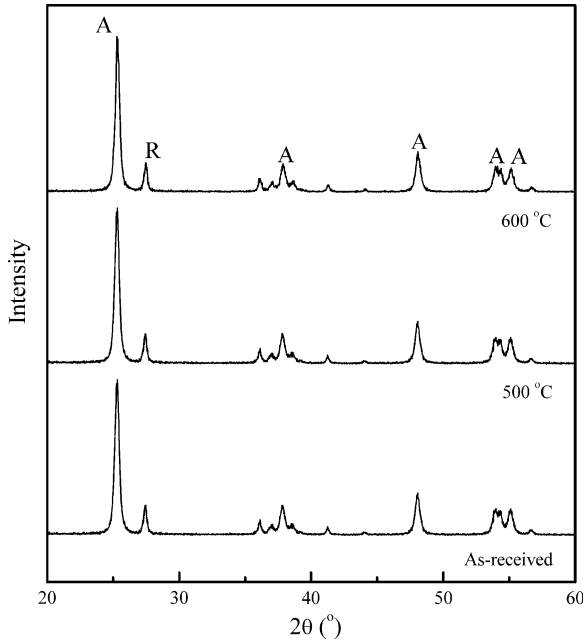

Fig. 4 XRD patterns of the as-received P25 powder and the P25 powder annealed at 500 °C and 600 °C. (A is referred to anatase phase, and R to rutile phase)

to the sufficiently filling of the particles to rough coating surface. This is evident from the surface morphology shown in Fig. 3b. Subsequently, there were no visible large interparticle pores in the coating. Only small pores mainly in size of 5-40 nm were present in the coating. The size of pores was in the same scale as primary P25 particle size.

XRD analysis revealed that the phase structure was not significantly influenced when annealing treatment was carried out at temperature lower than 600 °C. All coatings were composed of 85% anatase phase, which is superior to rutile phase as a photocatalyst.

It was clearly found from the photocatalytic experiment that the photocatalytic activity of the coating was enhanced by annealing treatment at temperatures of 400-500 °C. Some investigators reported that the interaction between anatase phase and rutile phase can increase the photocatalytic activity of TiO_2 in mixed phase (Ref 23-26). Possibly, the enhancement of the reactivity in this study may benefit from better interaction between anatase phase and rutile phase resulting from annealing treatment.

It was also noticed that the coating deposited with the composite powder presented much higher activity than that deposited with the primary P25 nanoparticles as both the coatings were annealed at the same temperature of 600 °C. It is known that photocatalysis is a surface property of TiO_2 semiconductor. The activity is influenced by surface area. There must be enough contaminants transporting into the inner coating part through the pores in the coating. Consequently, the higher transportation of contaminants into the coating and that of resultants outside the coating will lead to more surface area being photocatalytically active. With the coating deposited with the

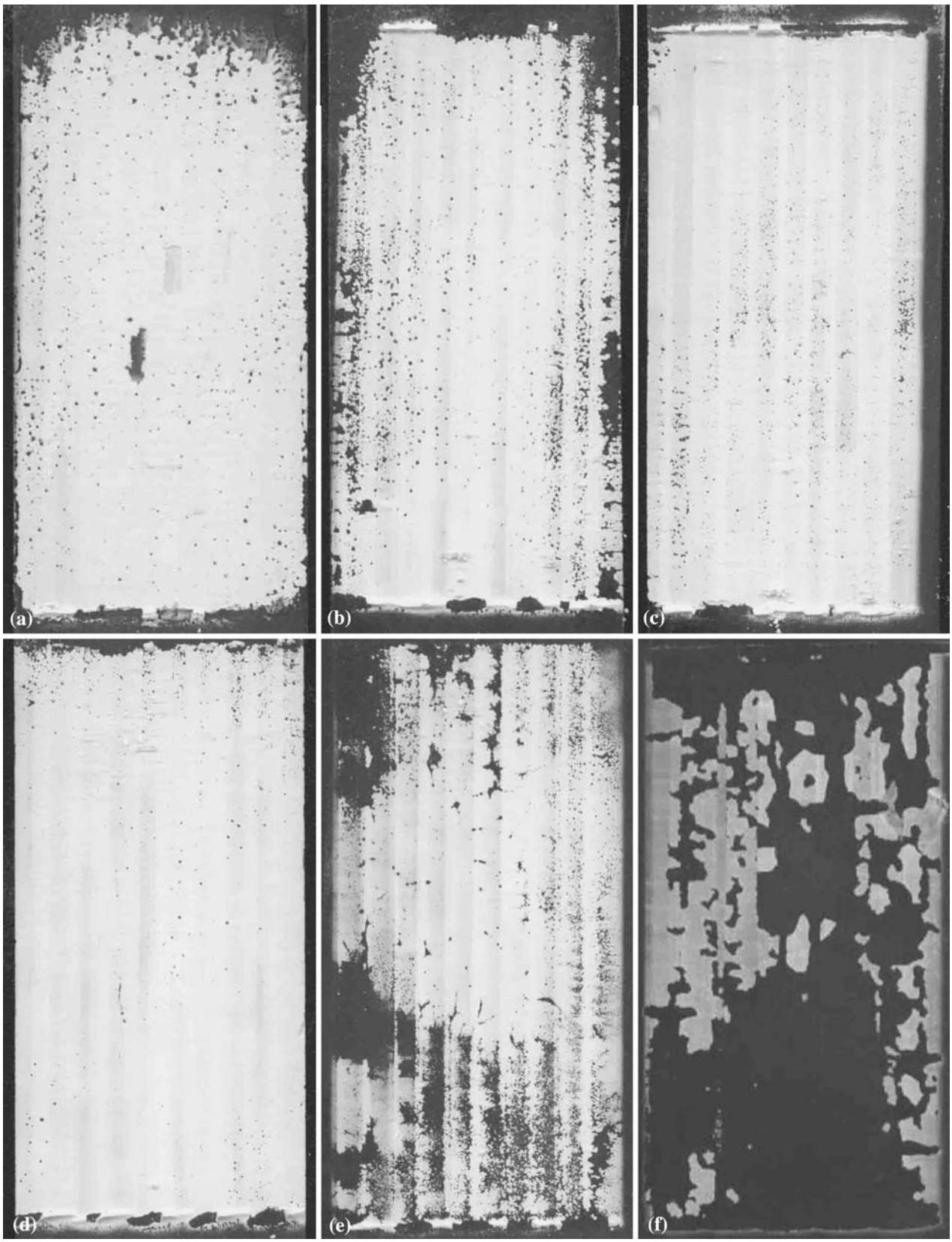

Fig. 5 Surface morphologies of the coatings annealed at different temperatures after ultrasonic cleaning. (a) 300 °C, (b) 400 °C, (c) 450 °C, (d) 500 °C, and (e) 600 °C for the coatings deposited with composite powder, (f) 600 °C for the coating deposited with primary P25

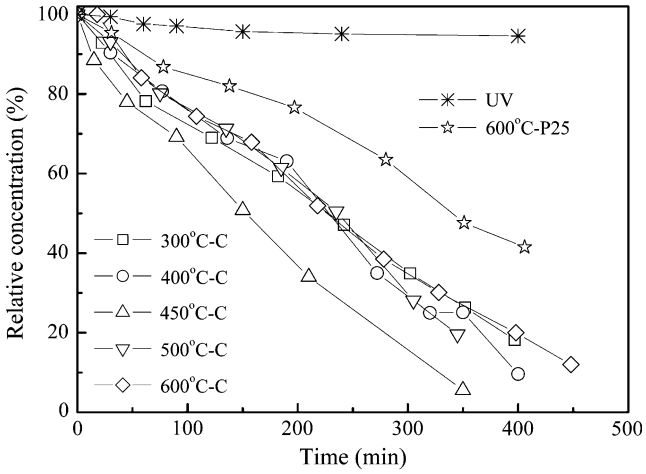

Fig. 6 Change of phenol concentration with the radiation time using TiO_2 coatings. (UV is referred to the blank reaction under UV illumination and without TiO_2 catalyst, C is referred to coatings deposited with the composite powder, and P25 to coating deposited with the primary P25 powder.)

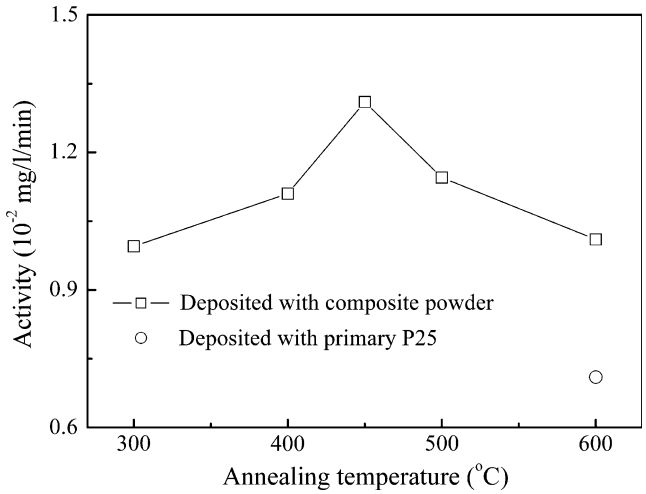

Fig. 7 Influence of annealing temperature on photocatalytic activity of TiO_2 coating

primary nanoparticles, only small pores were present. Contaminants transport into the inner coating through those small pores and then are involved in photocatalysis. With the coating deposited with the composite powder, both small pores and large pores were present in the coating. Contaminants can much more easily transport into the inner coating; therefore, the difference in the activity of the two coatings was attributed to the existence of large pores in the coatings.

5. Conclusions

The nanoTiO_2 photocatalytic coating was deposited through vacuum cold spray using both the composite powder and nanoTiO_2 powder. It was found that the photocatalytic activity of the coating deposited by the composite powders was significantly influenced by annealing temperature. The photocatalytic activity of the nanoTiO_2 coating was increased with the increase of annealing temperature from 300 to 450 °C and then tended to decrease with further increase of temperature to 600 °C. A better adhesion was achieved when the coating was annealed at temperature from 450 to 500 °C. The adhesion of the coatings deposited with the composite powder was better than the primary nanoTiO_2 powder. It was found that the TiO_2 coating deposited with the composite powder presented a higher phocatalytic activity than that deposited with the primary nanoparticles. Possibly, the high activity is attributed to the existence of large pores that benefits the contaminants transportation in the porous coating. The present results suggest that the nanostructured TiO_2 coating deposited through vacuum cold spray is a promising photocatalyst in the application to water purification.

Acknowledgment

The project was supported by the National Natural Science Foundation of China (Grant No.: 50602035).

References

1. A. Fujishima and K. Honda, Electrochemical Photolysis of Water at a Semiconductor Electrode, *Nature*, 1972, **238**, p 37-38
2. D.F. Ollis and H. Al-Ekabi, Photocatalytic Purification and Treatment of Water and Air. Elsevier, Amsterdam, 1993
3. R.P. Steijn, Friction and Wear of Rutile Crystal, *Am. Soc. Lubr. Eng. Trans.*, 1969, **12**, p 21-23
4. B. O'Regan and M. Gratzel, A Low-cost, High-efficiency Solar Cell Based on Dye-sensitized Colloidal TiO_2 Films, *Nature*, 1991, **353**, p 737-740
5. S.Y. Dai, K.J. Wang, J. Weng, Y.F. Sui, Y. Huang, S.F. Xiao, S.H. Chen, L.H. Hu, F.T. Kong, X. Pan, C.W. Shi, and L. Guo, Design of DSC Panel with Efficiency More than 6%, *Solar Energy Mater. Solar Cells*, 2005, **85**, p 447-455
6. Z.S. Wang, H. Kawauchi, T. Kashima, and H. Arakawa, Significant Influence of TiO_2 Photoelectrode Morphology on the Energy Conversion Efficiency of N719 Dye-sensitized Solar Cell, *Coord. Chem. Rev.*, 2004, **248**, p 1381-1389
7. S.-Q. Fan, C.-J. Li, C.-X. Li, G.-J. Liu, L.-Z. Zhang, and G.-J. Yang, Primary Study of Performance of Dye-sensitized Solar Cell of NanoTiO_2 Coating by Vacuum Cold Spraying, *Mater. Trans.*, 2006, **47**, p 1703-1709
8. M. Bideau, B. Claudel, C. Dubien, L. Faure, and H. Kazouan, On the ''Immobilization'' of Titanium Dioxide in the Photocatalytic Oxidation of Spent Waters, *J. Photocatal. Photobiol. A*, 1995, **91**, p 137-144
9. F.X. Ye, A. Ohmori, and C.J. Li, New Approach to Enhance the Photocatalytic Activity of Plasma Sprayed TiO_2 Coatings Using p-n Junctions, *Surf. Coat. Technol.*, 2004, **184**, p 233-238
10. F.X. Ye, A. Ohmori, and C.-J. Li, Photoresponse and Donor Concentration of Plasma-Sprayed TiO_2 and TiO_2-ZnO Electrodes, *J. Thermal Spray Technol.*, 2005, **14**, p 530-535
11. F.-L. Toma, D. Sokolov, G. Bertrand, D. Klein, C. Coddet, and C. Meunier, Comparison of the Photocatalytic Behavior of TiO_2 Coatings Elaborated by Different Thermal Spraying Processes, *J. Thermal Spray Technol.*, 2006, **15**, p 576-581
12. F.-L. Toma, G. Bertrand, S.O. Chwa, C. Meunier, D. Klein, and C. Coddet, Comparative Study on the Photocatalytic Decomposition of Nitrogen Oxides Using TiO_2 Coatings Prepared by

Conventional Plasma Spraying and Suspension Plasma Spraying, *Surf. Coat. Technol.*, 2006, **200**, p 5855-5862
13. C.-J. Li, G.-J. Yang, Y.-Y. Wang, C.-X. Li, F.-X. Ye, and A. Ohmori, Phase Formation during High Velocity Oxy-Fuel Spraying of TiO_2 Coatings, *Mater. Trans.*, 2006, **47**, p 1690-1696
14. G.-J. Yang, C.-J. Li, Y.-Y. Wang, and C.-X. Li, Dominant Microstructural Feature over Photocatalytic Activity of High Velocity Oxy-fuel Sprayed TiO_2 Coating, *Surf. Coat. Technol.*, Available online http://www.sciencedirect.com, 25 April 2007
15. C.-J. Li, G.-J. Yang, X.-C. Huang, W.-Y. Li, and A. Ohmori, Formation of TiO_2 Photocatalyst through Cold Spraying. Thermal Spray Solutions: Advances in Technology and Application, D. Hofe, Ed., Düsseldorg: DVS, 2004, p 315-319
16. C.-J. Li, G.-J. Yang, and Z. Wang, Formation of Nanostructured TiO_2 by Flame Spraying with Liquid Feedstock, *Mater. Lett.*, 2003, **57**, p 2130-2134
17. G.-J. Yang, C.-J. Li, and Y.-Y. Wang, Phase Formation of Nano-TiO_2 Particles during Flame Spraying with Liquid Feedstock, *J. Thermal Spray Technol.*, 2005, **14**, p 480-486
18. G.-J. Yang, C.-J. Li, C.-X. Li, Y.-Y. Wang, and X.-C. Huang, Effect of Cu^{2+} Doping on Photocatalytic Performance of Liquid Flame Sprayed TiO_2 Coatings, *J. Thermal Spray Technol.*, 2006, **15**, p 582-586
19. F.-L. Toma, G. Bertrand, D. Klein, C. Coddet, and C. Meunier, Nanostructured Photocatalytic Titania Coatings Formed by Suspension Plasma Spraying, *J. Thermal Spray Technol.*, 2006, **15**, p 587-592
20. M. Ichiki, J. Akedo, A. Schroth, R. Maeda, and Y. Ishikawa, X-ray Diffraction and Scanning Electron Microscopy Observation of Lead Zirconate Thick Film Formed by Gas Deposition Method, *Jpn. J. Appl. Phys.*, 1997, **36**, p 5815-5819
21. J. Akedo and M. Lebedev, Piezoelectric Properties and Poling Effect of $Pb(Zr,Ti)O_3$ Thick Films Prepared for Micro-actuators by Aerosol Deposition, *Appl. Phys. Lett.*, 2000, **77**, p 1710-1712
22. S.-Q. Fan, G.-J. Yang, C.-J. Li, G.-J. Liu, C.-X. Li, and L.-Z. Zhang, Characterization of Microstructure of Nano-TiO_2 Coating Deposited by Vacuum Cold Spraying, *J. Thermal Spray Technol.*, 2006, **15**, p 513-517
23. D.C. Hurum, A.G. Agrios, K.A. Gray, T. Rajh, and M.C. Thurnauer, Explaining the Enhanced Photocatalytic Activity of Degussa P25 Mixed-phase TiO_2 using EPR, *J. Phys. Chem. B*, 2003, **107**, p 4545-4549
24. T. Ohno, K. Sarukawa, K. Tokieda, and M. Matsumura, Morphology of a TiO_2 Photocatalyst (Degussa, P-25) Consisting of Anatase and Rutile Crystalline Phase, *J. Catal.*, 2001, **203**, p 82-86
25. R.I. Bickley, T. Gonzalez-Carreno, J.S. Lees, L. Palmisano, and R.J.D. Tilley, A Structural Investigation of Titanium Dioxide Photocatalysts, *J. Solid State Chem.*, 1991, **92**, p 178-190
26. T. Ohno, K. Tokieda, S. Higashida, and M. Matsumura, Synergism between Rutile and Anatase TiO_2 Particles in Photocatalytic Oxidation of Naphthalene, *Appl. Catal. A*, 2003, **244**, p 383-391